Entanglement of Two Superconducting Qubits in a Waveguide Cavity via Monochromatic Two-Photon Excitation

S. Poletto, Jay M. Gambetta, Seth T. Merkel, John A. Smolin, Jerry M. Chow, A. D. Córcoles, George A. Keefe, Mary B. Rothwell, J. R. Rozen, D. W. Abraham, Chad Rigetti, and M. Steffen

IBM T.J. Watson Research Center, Yorktown Heights, New York 10598, USA

(Received 13 August 2012; published 11 December 2012)

We report a system where fixed interactions between noncomputational levels make bright the otherwise forbidden two-photon $|00\rangle \rightarrow |11\rangle$ transition. The system is formed by hand selection and assembly of two discrete component transmon-style superconducting qubits inside a rectangular microwave cavity. The application of a monochromatic drive tuned to this transition induces two-photon Rabi-like oscillations between the ground and doubly excited states via the Bell basis. The system therefore allows all-microwave two-qubit universal control with the same techniques and hardware required for single qubit control. We report Ramsey-like and spin echo sequences with the generated Bell states, and measure a two-qubit gate fidelity of $F_g = 90\%$ (unconstrained) and 86% (maximum likelihood estimator).

DOI: 10.1103/PhysRevLett.109.240505 PACS numbers: 03.67.Bg, 03.67.Ac, 42.50.Pq, 85.25.−j

Recent improvements in the qubit coherence times [1,2] and fidelities of one- and two-qubit gates [3,4] for superconducting circuits have fed optimism for large scale quantum information processing with these devices. One-qubit gates are typically performed with exclusively microwave control pulses [5,6]. These techniques were recently extended to two-qubit gates with the cross-resonance scheme [3,7–10]. Earlier work required dc tuning of qubit frequencies [11–14]. In particular, Refs. [15–18] exploited interactions of higher levels of the quantum circuits to produce an effective interaction in the computational basis; the physics of higher levels has also been exploited elsewhere in quantum computing [19]. Superconducting circuits can be designed to have particular values of their energy transitions and associated derivatives. In this Letter we use this capability—in conjunction with the modularity of individual discrete devices within a three-dimensional enclosure—to implement a new all-microwave two-qubit gate induced by the direct drive of the $|00\rangle \rightarrow |11\rangle$ transition, which would be forbidden were it not for the interaction of higher levels.

This transition is impossible in harmonic systems and is a small third order interaction in coupled qubit systems. However, as we show, it can be made bright in coupled multilevel systems when the qubit-qubit detuning approaches the anharmonicity. This transition has also been observed spectroscopically for a two-level system coupled to a phase qubit [20]. A microwave pulse tuned to this two-photon transition induces an effective Hamiltonian which implements a rotation in the $\{|00\rangle, |11\rangle\}$ subspace whose angle is set by the action of the pulse, allowing the direct generation of entanglement from the ground state. The gate is similar to that proposed by Mølmer and Sorenson [21], which is a bichromatic two-photon excitation and has become commonplace in trapped ion quantum computing [22,23]. As such, it holds promise for the direct generation of entangled states of larger multiqubit systems.

The device we study is based on a three-dimensional circuit QED architecture [1]. We leverage the modularity of this design to build up a multiqubit system from individual discrete components, each of which is independently designed, tested, characterized—and selected—for optimal parameters to realize this effect.

We use this procedure to implement a two-transmon circuit-QED system [24,25] described by the Hamiltonian ($\hbar = 1$)

$$H = \left(\omega_1 - \frac{\delta_1}{2}\right)a^\dagger a + \frac{\delta_1}{2}(a^\dagger a)^2 + \left(\omega_2 - \frac{\delta_2}{2}\right)b^\dagger b + \frac{\delta_2}{2}(b^\dagger b)^2 + J(a^\dagger b + a b^\dagger) + \Omega\cos(\omega_d t + \phi)(a + a^\dagger + \lambda b + \lambda b^\dagger), \quad (1)$$

where $\omega_{1(2)}$ is the $|0\rangle \rightarrow |1\rangle$ transition frequency of transmon 1 (2); $\delta_{1(2)}$ is the anharmonicity of transmon 1 (2); J is the effective strength of the exchange interaction between transmons; Ω is the amplitude of the applied microwave field of frequency ω_d and phase ϕ; λ is the coupling coefficient of the driving signal to transmon 2 normalized to transmon 1 (in our case $\lambda \simeq 1$); and a (b) are the annihilation operators for transmon 1 (2).

In a frame rotating with a drive of frequency ω_d near the midpoint of ω_1 and ω_2 the states $|00\rangle$ and $|11\rangle$ form a low energy manifold. As shown in the Supplemental Material [26] we can use a sequence of Schrieffer-Wolff transformations which remove the coupling between this lower energy manifold and the remainder of the Hilbert space. Doing so results in an effective Hamiltonian that both couples $|00\rangle \rightarrow |11\rangle$ and produces a Stark shift of each of the four computational states. By adjusting ω_d it is possible to make the Stark shifted $|00\rangle$ and $|11\rangle$ levels degenerate in

the rotating frame, and thereby generate an effective unitary $U = U_B U_{ZZ} U_{IZ-ZI}$, where

$$U_B(t) = \begin{pmatrix} \cos\left(\frac{\Omega_B t}{2}\right) & 0 & 0 & -ie^{-2i\phi}\sin\left(\frac{\Omega_B t}{2}\right) \\ 0 & 1 & 0 & 0 \\ 0 & 0 & 1 & 0 \\ -ie^{2i\phi}\sin\left(\frac{\Omega_B t}{2}\right) & 0 & 0 & \cos\left(\frac{\Omega_B t}{2}\right) \end{pmatrix} \tag{2}$$

with

$$\Omega_B = \frac{-2J\Omega^2(-J\lambda(\delta_1+\delta_2)+\lambda^2\delta_2(\delta_1+\Delta)+\delta_1(\delta_2-\Delta))}{(\delta_2-\Delta)(\delta_1+\Delta)\Delta^2} \tag{3}$$

and $\Delta = \omega_1 - \omega_2$. The operator U_B generates a Rabi-like rotation at angular frequency Ω_B about an axis defined by the azimuthal angle $\varphi = 2\phi + \pi/2$ in the equatorial plane of a Bloch sphere whose poles are $|00\rangle$ and $|11\rangle$. The remaining transformations $U_{ZZ} = \exp(-i\alpha_{zz} ZZt/4)$ and $U_{IZ-ZI} = \exp(-i\alpha_-(IZ - ZI)t/4)$ commute with U_B and, despite the rather complicated equations for α_{zz} and α_-, can be left out and corrected with post processing or refocusing techniques.

A gate that is locally equivalent to iSWAP is implemented by choosing a time $t = \pi/\Omega_B$. We refer to this gate as the bSWAP. This Clifford gate, along with single qubit unitaries, forms a universal set of gates for fault-tolerant computation. With a time $t = \pi/2\Omega_B$ it implements instead a $\pi/2$ rotation (the $\sqrt{\text{bSWAP}}$ gate), which when applied to the ground state produces the Bell state $\frac{1}{\sqrt{2}}(|00\rangle + e^{i\varphi}|11\rangle)$. This gate, accordingly, is locally equivalent to $\sqrt{\text{iSWAP}}$.

The magnitude of Ω_B has some interesting limits. In the limit of $\delta_i \ll \Delta$ (the harmonic oscillator limit) $\Omega_B \to 0$ as expected, while for $\delta_i \gg \Delta$ (pure qubit limit) it reduces to $\Omega_B = -2J\Omega^2(1+\lambda)/\Delta^2$ and for typical values of Ω, J, and Δ it is extremely small, explaining why this effect has not previously been exploited. The relevant case for this work is the limit in which Δ approaches either $-\delta_1$ or δ_2 since the rate passes through a resonance and becomes large. Such condition is met when the $|0\rangle \to |1\rangle$ transition of one transmon approaches the $|1\rangle \to |2\rangle$ transition of the other. As a consequence, the energy level $|11\rangle$ is close to $|02\rangle$ and the leakages from the computational subspace are increased. It is essentially this leakage rate that determines the maximum Ω_B with which the gate can be operated. In this work δ_2 is close to Δ which results in an enhancement of Ω_B by a multiplicative factor of $\delta_2/2(\delta_2 - \Delta)$ relative to the pure qubit limit [27].

The enclosure, machined from bulk oxygen-free high thermal conductivity copper subsequently sputtered with aluminum, has an interior volume of $(15.5 \times 18.6 \times 4.2)$ mm^3. Two commercial bulkhead SMA connectors provide an input and output port to introduce drive signals and perform measurements. The transmons and the method of applying control pulses through the enclosure are described in Refs. [1,2]. Transmons are fabricated on individual sapphire chips and, following independent pre-characterization, are selected to match the resonance conditions described earlier (Table I). The two chips are mounted symmetrically into the cavity, each 2.1 mm away from the maximum of the TE_{101} mode [see Fig. 1(a)].

The sample is shielded by a Cryoperm can filled with Eccosorb® foam to suppress spurious thermal radiation [28]. The signal transmitted by the cavity passes through two circulators and a low-pass filter at base temperature prior to being amplified by a low noise cryogenic HEMT amplifier at 2.8 K and further amplified at room temperature. The information about the state of the system is extracted by a joint readout technique [29] with heterodyne detection by down-conversion.

A spectroscopic measurement of the coupled system is shown in Fig. 1(c). The strength of the two-photon transition associated with U_B is increased by a factor of 15 compared to the pure qubit limit, greatly enhancing its visibility. The ZZ coupling is $E_{11} - E_{10} - E_{01} \simeq 90$ kHz and is small enough to allow for high fidelity single qubit gates with minimal pulse shaping.

Driving the $|00\rangle \to |11\rangle$ transition generates coherent oscillations between the two states [see Fig. 2(a)]. The measured oscillation frequency Ω_B versus the amplitude of the microwave driving signal [Fig. 2(b)] has the quadratic dependence expected from Eq. (3) for small amplitudes. We ascribe the discrepancy observed at higher amplitudes to the higher levels of the system. To confirm this, we did numerical simulations including the first 3

TABLE I. Measured properties of the two transmons independently measured (lines 1 and 2), as well as when placed inside the enclosure (lines 3 and 4).

Transmon	Size pads (μm^2)	E_{01} (GHz)	E_{12} (GHz)	T_1 (μs)	T_2^*(μs)	E_j/E_c
A5 (ind)	500×500	4.4513	4.2130	26	16	48
A8 (ind)	600×300	4.7013	4.4616	26	13	53
A5 (coup)	500×500	4.3796	4.1403	38	29.5[a]	47
A8 (coup)	600×300	4.61368	4.3709	32	16	50

[a]we report here the T_2 value obtained with a spin echo procedure since we observed beating on Ramsey oscillations.

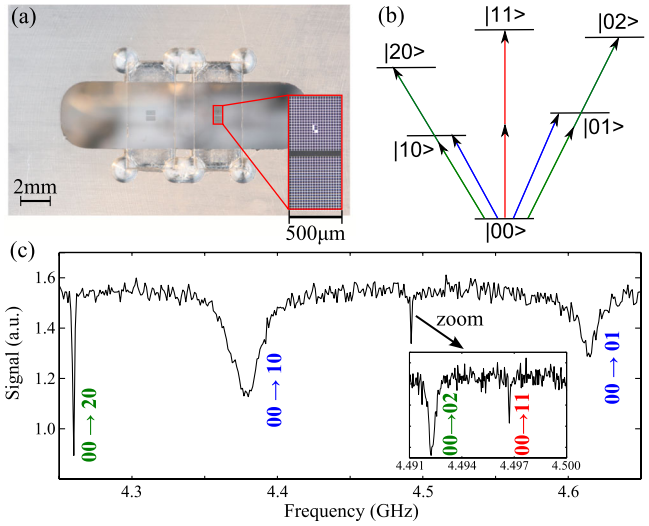

FIG. 1 (color online). (a) Picture of half a cavity with two independent transmons mounted. The inset is a magnified image of one of the transmons. (b) Energy diagram of the system. Single and two-photon transitions are depicted, respectively, with one and two arrows. (c) Spectrum of the system. The activation of the transition $|00\rangle \rightarrow |11\rangle$ requires more power than any other transitions here measured because it is a second order transition further reduced by a factor of J/Δ. The dressed cavity resonance frequency is at 11.7781 GHz.

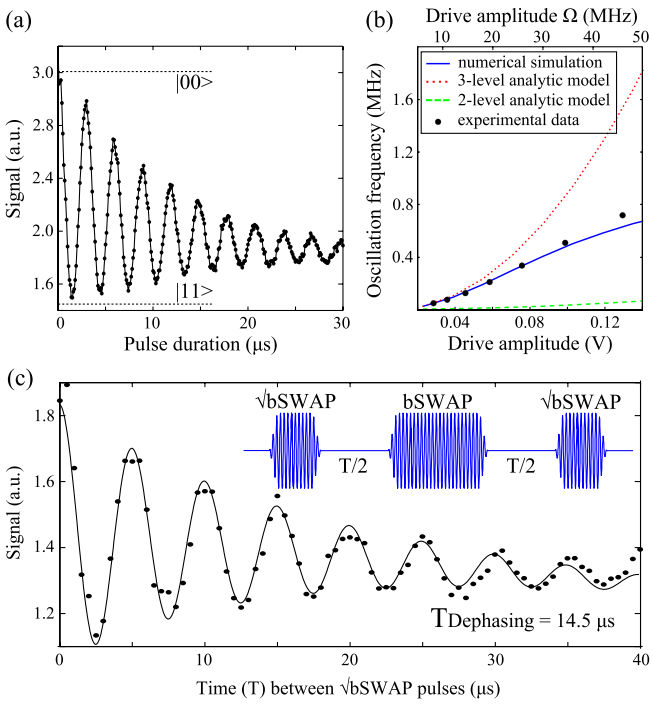

FIG. 2 (color online). (a) Two-photon coherent oscillation between the states $|00\rangle$ and $|11\rangle$. The oscillation saturates at approximately 1/4 of its visibility because in the steady state all four states $|00\rangle$ through $|11\rangle$ are equally populated. (b) Oscillation frequency versus driving amplitude. Black dots are experimental data, the solid blue line is a multilevel numerical simulation, the dotted red line is derived from perturbation theory of coupled multilevel systems, and the dashed green line is from perturbation theory applied to coupled two-level systems. We ascribe the discrepancy observed at large amplitudes to the higher levels of the system, an effect that is captured by the numerical simulation. (c) Evaluation of the dephasing time of the Bell state with a spin-echo experiment. The refocusing bSWAP is symmetrically placed between two $\sqrt{\text{bSWAP}}$ gates (inset), and the oscillation is experimentally induced by linearly ramping the phase of the last pulse in time.

levels; the results agree quantitatively with our experimental data.

Full state and process tomography on this system requires three microwave tones to generate the two single qubit gates and the U_B transformation. Each tone has a phase, and it is necessary to maintain the phase relationship between φ (the phase defining U_B) and the single qubit phases. We approach this problem by using only two microwave sources and single sideband modulation. One microwave source is at frequency $\nu_1 = 4.49368$ GHz and generates the single qubit pulses employing sideband modulation at -114 and 120 MHz to match the qubit frequencies. To prevent leakage from the computational subspace the pulses have a duration of 200 ns and a Gaussian shape with standard deviation $\sigma = 50$ ns. The other microwave source is at frequency $\nu_2 = 4.59\,698$ GHz and generates U_B, or the $\sqrt{\text{bSWAP}}$ gate, also via sideband modulation at -100 MHz. To ensure proper phase relationship between individual experiments making up an ensemble average, we obey the experimental repetition rate of $m/[2(\nu_1 - \nu_2)]$ where m is an integer.

A Bell state of the form $\frac{1}{\sqrt{2}}(|00\rangle + e^{i\varphi}|11\rangle)$ is produced by stopping the driven evolution under U_B at the time $t = \pi/2\Omega_B$ which in this experiment is 800 ns. Tomographic reconstruction of the prepared state is obtained by measuring all 36 combinations of the single qubit rotations $\{I, X_\pi, X_{\pm\pi/2}, Y_{\pm\pi/2}\}^{\otimes 2}$ (with $X_\alpha[Y_\alpha]$ being $X[Y]$ rotations of α radians). Then either a linear inversion (by a pseudo inverse) or a maximum likelihood estimation (MLE) [3,30] is used to reconstruct the quantum state.

We used this procedure to create and characterize the Bell states $\frac{1}{\sqrt{2}}(|00\rangle + |11\rangle)$ and $\frac{1}{\sqrt{2}}(|00\rangle + i|11\rangle)$ [Figs. 3(a) and 3(b)]. Measured values for the state fidelities are >99%.

The angle φ is completely defined by the relative phase ϕ between the two microwave sources. In Fig. 3(c) the expectation value of the two-qubit Pauli operators are plotted versus the relative phase between microwave sources. Only the operators XX, XY, YX, YY have oscillating expectation values, clearly indicating a transfer of information between real and imaginary part. The periodicity is double the relative phase between the two microwave sources as expected from Eq. (2).

The ability of the $\sqrt{\text{bSWAP}}$ gate to generate a Bell state with a single pulse allows for a measurement of the Bell

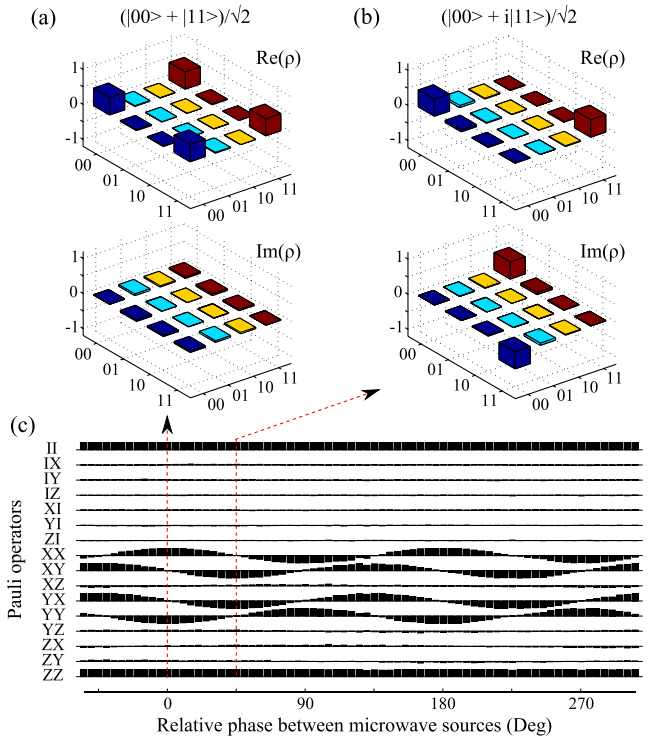

FIG. 3 (color online). (a)–(b) Tomographic reconstruction of the two Bell states $\frac{1}{\sqrt{2}}(|00\rangle + |11\rangle)$ and $\frac{1}{\sqrt{2}}(|00\rangle + i|11\rangle)$. (c) Expectation value of the two-qubit Pauli operators versus the relative phase between microwave sources used to generate the $\sqrt{\text{bSWAP}}$ gate and the single qubit pulses.

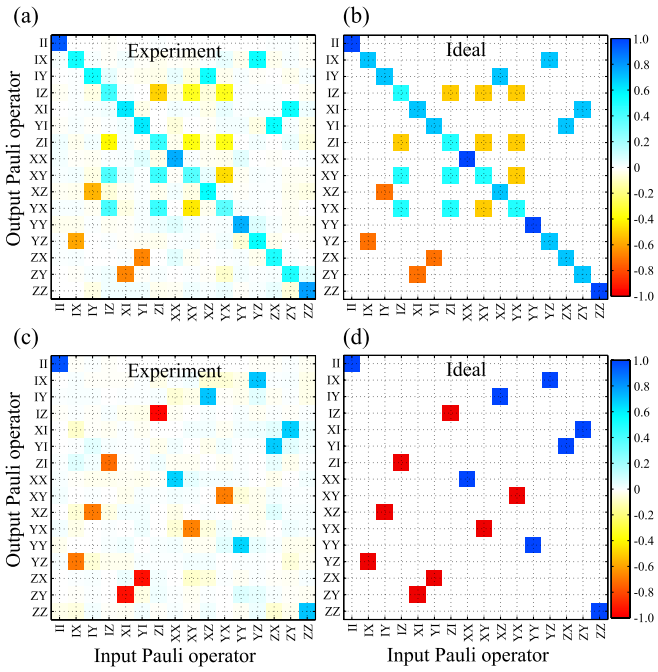

FIG. 4 (color online). Experimental [(a) and (c)] and ideal [(b) and (d)] Pauli transfer matrices for the $\sqrt{\text{bSWAP}}$ [(a) and (b)] and the bSWAP [(c) and (d)] gates.

state dephasing time with a spin echo technique. By implementing the pulse sequence in the inset of Fig. 2(c), we measured a Bell state dephasing time of 14.5 μs [Fig. 2(c)].

Quantum process tomography of the $\sqrt{\text{bSWAP}}$ and bSWAP gates is done by performing a set of 36×36 measurements corresponding to full state tomography on the 36 different input states generated by $\{I, X_{\pi}, X_{\pm\pi/2}, Y_{\pm\pi/2}\}^{\otimes 2}$. The Pauli transfer matrix $\mathcal{R}$ [3] is calculated by either a linear inversion or a MLE, and the gate fidelity is evaluated from the equation $F_g = (\text{Tr}[\mathcal{R}^{\dagger}\mathcal{R}] + 4)/20$ [3]. Figures 4(a) and 4(b) are, respectively, the measured and ideal Pauli transfer matrices $\mathcal{R}$ for the $\sqrt{\text{bSWAP}}$ gate. The measured gate fidelity is $F_{\sqrt{\text{bSWAP}}} = 90\%$ (raw) and 86% (MLE).

The main source of gate error is a reduction in the dephasing time T_2^* during the experiment induced by the comparatively high power pulse used for the $\sqrt{\text{bSWAP}}$ gate. This is fit very well by simulations of the Pauli transfer matrix with a T_2^* of 4 μs, but more importantly can be observed directly in the experiment as follows. We measure T_{echo} of qubit A5 in a spin-echo experiment where during the delays we drive the system with a pulse far detuned from any transition but of the same amplitude as that used for the $\sqrt{\text{bSWAP}}$ gate. These experiments gave $T_2 = 6.8$ μs as compared to $T_2 = 29.5$ μs in the absence of the drive. We postulate that this deterioration of the dephasing time is due to thermal photons produced in the 20 dB attenuator at 10 mK. These photons produce a fluctuating cavity population and dephase the qubit as described in [2], from which we estimated a thermal photon number of 0.1 emitted by sources (the central pin of the bulkhead SMA connectors used as input and output ports) at 240 mK. Experiments with non-dissipative attenuation techniques are underway.

Finally, we perform quantum process tomography of the two qubit Clifford operator bSWAP (Figs. 4(c) and 4(d)). The measured gate fidelity is $F_{\text{bSWAP}} = 87.3\%$ (raw) and 80% (MLE).

In conclusion, we have introduced a new two-qubit gate based on the $|00\rangle \rightarrow |11\rangle$ transition, which is forbidden but can be driven by a two photon interaction. Because of the higher levels of our system this rate can be greatly enhanced when the $|0\rangle \rightarrow |1\rangle$ transition of one transmon approaches the $|1\rangle \rightarrow |2\rangle$ transition of the other transmon. The resulting gate creates a maximally entangled state between two qubits directly from the ground state and, like the single qubit gates, is implemented with a single microwave pulse of defined duration, amplitude and phase. Together with single qubit gates this generates a universal set of gates for quantum computation. Based on the interactions we have shown here, we believe additional two-qubit gate schemes are possible including, for example, off-resonance driving of the $|11\rangle \rightarrow |22\rangle$ transition. Further, we have shown it is possible to realize high-fidelity quantum gates and entangled states with discrete component superconducting qubits. This general approach may hold promise

as a complement to the established method of building prototype quantum processors with integrated quantum circuits.

We acknowledge fruitful discussions and contributions from David P. DiVincenzo, Zachary Dutton, Blake R. Johnson, Colm A. Ryan, Erik Lucero, and Douglas McClure as well as Mark Ketchen for his contributions in managing the program. We acknowledge support from IARPA under Contract No. W911NF-10-1-0324. All statements of fact, opinion or conclusions contained herein are those of the authors and should not be construed as representing the official views or policies of the U.S. Government.

[1] H. Paik *et al.*, Phys. Rev. Lett. **107**, 240501 (2011).
[2] C. Rigetti *et al.*, Phys. Rev. B **86**, 100506(R) (2012).
[3] J. M. Chow *et al.*, Phys. Rev. Lett. **109**, 060501 (2012).
[4] E. Magesan *et al.*, Phys. Rev. Lett. **109**, 080505 (2012).
[5] J. M. Martinis, S. Nam, J. Aumentado, and C. Urbina, Phys. Rev. Lett. **89**, 117901 (2002).
[6] A. Wallraff, D. I. Schuster, A. Blais, L. Frunzio, J. Majer, M. H. Devoret, S. M. Girvin, and R. J. Schoelkopf, Phys. Rev. Lett. **95**, 060501 (2005).
[7] G. S. Paraoanu, Phys. Rev. B **74**, 140504 (2006).
[8] C. Rigetti and M. Devoret, Phys. Rev. B **81**, 134507 (2010).
[9] P. C. de Groot, J. Lisenfeld, R. N. Schouten, S. Ashhab, A. Lupaşcu, C. J. P. M. Harmans, and J. E. Mooij, Nat. Phys. **6**, 763 (2010).
[10] J. M. Chow *et al.*, Phys. Rev. Lett. **107**, 080502 (2011).
[11] M. Steffen, M. Ansmann, R. C. Bialczak, N. Katz, E. Lucero, R. McDermott, M. Neeley, E. M. Weig, A. N. Cleland, and J. M. Martinis, Science **313**, 1423 (2006).
[12] J. Majer *et al.*, Nature (London) **449**, 443 (2007).
[13] R. C. Bialczak *et al.*, Nat. Phys. **6**, 409 (2010).
[14] A. Dewes, F. Ong, V. Schmitt, R. Lauro, N. Boulant, P. Bertet, D. Vion, and D. Esteve, Phys. Rev. Lett. **108**, 057002 (2012).
[15] F. W. Strauch, P. R. Johnson, A. J. Dragt, C. J. Lobb, J. R. Anderson, and F. C. Wellstood, Phys. Rev. Lett. **91**, 167005 (2003).
[16] L. DiCarlo *et al.*, Nature (London) **460**, 240 (2009).
[17] T. Yamamoto *et al.*, Phys. Rev. B **82**, 184515 (2010).
[18] L. DiCarlo, M. D. Reed, L. Sun, B. R. Johnson, J. M. Chow, J. M. Gambetta, L. Frunzio, S. M. Girvin, M. H. Devoret, and R. J. Schoelkopf, Nature (London) **467**, 574 (2010).
[19] B. P. Lanyon, M. Barbieri, M. P. Almeida, T. Jennewein, T. C. Ralph, K. J. Resch, G. J. Pryde, J. L. O'Brien, A. Gilchrist, and A. G. White, Nat. Phys. **5**, 134 (2009).
[20] P. Bushev, C. Müller, J. Lisenfeld, J. H. Cole, A. Lukashenko, A. Shnirman, and A. V. Ustinov, Phys. Rev. B **82**, 134530 (2010).
[21] A. Sørensen and K. Mølmer, Phys. Rev. A **62**, 022311 (2000).
[22] J. Benhelm, G. Kirchmair, C. F. Roos, and R. Blatt, Nat. Phys. **4**, 463 (2008).
[23] T. Monz, P. Schindler, J. T. Barreiro, M. Chwalla, D. Nigg, W. A. Coish, M. Harlander, W. Hänsel, M. Hennrich, and R. Blatt, Phys. Rev. Lett. **106**, 130506 (2011).
[24] J. Koch, T. M. Yu, J. Gambetta, A. A. Houck, D. I. Schuster, J. Majer, A. Blais, M. H. Devoret, S. M. Girvin, and R. J. Schoelkopf, Phys. Rev. A **76**, 042319 (2007).
[25] A. Blais, J. Gambetta, A. Wallraff, D. I. Schuster, S. M. Girvin, M. H. Devoret, and R. J. Schoelkopf, Phys. Rev. A **75**, 032329 (2007).
[26] See Supplemental Material at http://link.aps.org/supplemental/10.1103/PhysRevLett.109.240505 for a detailed description of the Schrieffer-Wolff transformation and the derivation of the two-photon gate.
[27] References [15–18] use a similar condition with fast flux tuning to generate two-qubit gates.
[28] A. D. Corcoles, J. M. Chow, J. M. Gambetta, C. Rigetti, J. R. Rozen, G. A. Keefe, M. B. Rothwell, M. B. Ketchen, and M. Steffen, Appl. Phys. Lett. **99**, 181 906 (2011).
[29] S. Filipp *et al.*, Phys. Rev. Lett. **102**, 200402 (2009).
[30] M. Paris and J. Řeháček, *Quantum State Estimation*, Lecture Notes in Physics (Springer, Berlin, 2004).